EEET ECOLOGICAL ENGINEERING & ENVIRONMENTAL TECHNOLOGY

Ecological Engineering & Environmental Technology, 2026, 27(10), 430–447
https://doi.org/10.12912/27197050/231652
ISSN 2719–7050, License CC-BY 4.0

Received: 2026.07.30
Accepted: 2026.08.31
Published: 2026.09.10

Structural control on groundwater hydrogeochemical evolution and recharge processes in the semi-arid Chemora Plain (northeastern Algeria): Integrated insights from hydrochemistry, stable isotopes and multivariate statistics

Amina Tahar Khelkhal[1*], Nafaa Brinis[1]

[1] Laboratory of Water Resources Mobilization and Management (LMGRE) Department of Geology, Institute of Earth and Universe Sciences, University of Batna 2, Algeria
* Corresponding author's e-mail: aminakhelkhal1@gmail.com

ABSTRACT

Understanding the factors controlling groundwater mineralization is essential for the sustainable management of water resources in semi-arid environments. This study investigates the hydrogeochemical functioning of the Chemora Plain aquifer (northeastern Algeria), where a Cretaceous structural ridge divides the alluvial basin into northern and southern hydrogeological compartments. A multidisciplinary dataset combining major-ion hydrochemistry, water hardness, mineral saturation indices, stable isotopes ($\delta^{18}O$ and $\delta^{2}H$), and principal component analysis (PCA) was used to test the hydrogeochemical significance of this structural organization. Electrical conductivity, hardness and major-ion distributions reveal differentiated groundwater evolution between the southern and northern compartments, while comparable EC values near the structural boundary indicate that the compartments are not completely isolated. Saturation indices show near-equilibrium conditions for carbonate minerals and persistent undersaturation with respect to gypsum, anhydrite and halite, supporting continued water–rock interaction and a potential contribution of evaporite dissolution to mineralization. Stable isotope compositions ($\delta^{18}O$ = −8.96 to −5.89‰; $\delta^{2}H$ = −54.98 to −39.10‰; d-excess = 7–17‰) indicate a predominantly meteoric recharge source with limited isotopic modification. PCA further identifies distinct hydrochemical associations for the northern and southern sectors, while shared variables indicate partial hydraulic connectivity. The integrated evidence supports a conceptual model in which the Fedjoudj–Bouarif Cretaceous ridge acts as a major structural threshold, whereas the western breach permits localized hydraulic exchange. The main contribution of this study is therefore the demonstration of a structurally controlled hydrogeochemical evolution in the Chemora aquifer through the convergence of independent geological, hydrochemical, isotopic and statistical evidence.

Keywords: structural compartmentalization, groundwater hydrochemistry, stable isotopes ($\delta^{18}O$–$\delta^{2}H$), water–rock interaction, principal component analysis, semi-arid aquifer.

INTRODUCTION

Groundwater represents a major source of water for domestic supply, irrigation and other uses in many semi-arid and arid regions, where limited and variable surface-water availability can increase dependence on groundwater resources. Groundwater-quality deterioration is therefore an important environmental and resource-management concern, particularly in regions where groundwater represents a major source of water supply (Gumbo and Kapenge, 2025; Ali et al., 2024). In semi-arid settings, increasing abstraction, recurrent drought and land-use pressure can amplify the risks of salinization and declining water quality.

In semi-arid environments, groundwater chemistry is controlled by a complex interaction between climate, geology, groundwater residence time, water-rock interactions, evaporation, and

human activities (Rezig et al., 2023; Hammadi et al., 2022; Appelo, Postma, 2004; Freeze, Cherry, 1979). Under limited recharge conditions, prolonged groundwater circulation enhances mineral dissolution and geochemical evolution, while intense evapotranspiration promotes salt concentration and progressive salinization, particularly within endorheic basins where groundwater naturally converges toward discharge areas (Hardie, Eugster, 1970; Drever, 1997; Yan, 2002). Understanding these processes is essential not only for evaluating groundwater quality but also for predicting its long-term evolution and suitability for agricultural use.

Hydrochemical investigations constitute one of the most effective tools for identifying the mechanisms controlling groundwater evolution. The distribution of major ions, hydrochemical facies, mineral saturation indices, and multivariate statistical analyses provides valuable information on mineral dissolution, ion exchange, evaporation, mixing processes, and groundwater flow dynamics (Hem, 1985; Appelo, Postma, 2004; Cloutier et al., 2008, Brinis et al., 2015). Nevertheless, hydrochemical data alone may not always distinguish between different recharge sources or identify the relative importance of evaporation and groundwater mixing.

Stable isotopes of oxygen ($\delta^{18}O$) and hydrogen ($\delta^{2}H$) have therefore become indispensable tracers in hydrogeological investigations because they preserve information on groundwater origin, recharge conditions, evaporation processes, and groundwater circulation pathways (Craig, 1961; Clark, Fritz, 1997; Kendall, McDonnell, 1998). Combined with hydrochemical analyses, stable isotopes considerably improve the understanding of groundwater evolution and allow the development of conceptual hydrogeological models capable of explaining spatial variations in groundwater quality.

The Chemora Plain, located in northeastern Algeria, is a semi-arid agricultural basin in which groundwater from Quaternary deposits supports irrigation. The plain contains a central Cretaceous structural relief separating two geomorphological depressions. Despite the socio-economic importance of the aquifer, previous studies have mainly focused on groundwater-quality assessment or irrigation suitability, while it remains unclear whether the central Cretaceous structural relief acts as an effective hydrogeological boundary, to what extent it separates groundwater circulation and hydrochemical evolution between the northern and southern parts of the plain, and whether the two compartments remain hydraulically connected through the structural breach identified in the western part of the ridge.

Previous studies have been conducted in the Chemora Plain and in neighboring plains, particularly the Remila Plain (Bezai et al, 2023, Aouidane et al., 2021; Ghodbane, 2018; Belkoum and Houha, 2017; Ghodbane et al., 2016,). However, to our knowledge, no previous investigation has integrated geological structural interpretation, hydrochemical characterization, mineral saturation modelling, stable isotope techniques and multivariate statistical analysis specifically to test the role of the Cretaceous structural threshold in groundwater compartmentalization and hydrogeochemical evolution within the Chemora aquifer. The scientific contribution of the present study therefore does not lie in the novelty of the individual analytical methods, which are well established, but in their convergence to constrain a previously insufficiently documented hydrogeological functioning model for this structurally complex semi-arid aquifer.

Therefore, this study aims to determine how the Cretaceous Fedjoudj–Bouarif structural threshold controls groundwater compartmentalization, recharge, flow pathways, and hydrogeochemical evolution in the Chemora Plain aquifer. Specifically, we test the hypothesis that the structural ridge separates the aquifer into hydrochemically differentiated compartments, while localized hydraulic connectivity may occur through structural discontinuities. We further hypothesize that the observed increase in groundwater mineralization is primarily related to differences in groundwater circulation, residence time, and water–rock interaction rather than to distinct recharge sources. To test these hypotheses, we (i) characterize groundwater chemistry and hardness, (ii) evaluate mineral saturation states, (iii) use δ18O and δ2H to constrain recharge origin and isotopic modification, and (iv) integrate these independent lines of evidence with multivariate statistics.

MATERIAL AND METHODS

Study area

The study area is located within the Chemora Plain in northeastern Algeria (Figure 1), between 35°31′–35°50′N and 6°30′–6°58′E, covering

approximately 459–486 km² and extending from 850 to 1100 m a.s.l. The plain extends across the wilayas of Batna and Oum El Bouaghi and includes the communes of Chemora, Boulhilet, Ain Kercha and Boughrara Saoudi, together with surrounding agricultural settlements. The study area was delineated using ArcGIS Desktop 10.8 (Esri, 2020), in the WGS 1984 UTM Zone 32N coordinate system, based on the Geological Map of Algeria, including the Ain El Ksar Sheet No. 173, Boulhilet Sheet No. 174, and Garaet Et Tarf Sheet No. 175, at a scale of 1:50,000. The boundaries were defined with reference to the available geological, topographic and administrative mapping, while the main geomorphological units and drainage network were identified from these cartographic sources. Geomorphologically, the plain belongs to the Aurès domain of the Atlas system and comprises two main depressions, the Chemora–Boulhilet basin to the north and the Chemora–Remila basin to the south, separated by the east–west-oriented Djebel Fedjoudj (1.248 m). These depressions form part of hydrographic sub-basins 07-04, 05 and 06 identified by the National Agency for Water Resources (ANRH) and are characterized by internal drainage, which is relevant to groundwater recharge and flow. Land use is predominantly agricultural, with intensive cereal cultivation, particularly wheat and barley, covering approximately 16,940 ha, while steppic rangelands occupy much of the remaining area. The regional climate is semi-arid, with a mean annual precipitation of 323.124 mm and a mean annual temperature of 13.71 °C, based on data from the Timgad meteorological station for 2005–2023. The combination of internal drainage, semi-arid climatic conditions and intensive agricultural activity makes the plain particularly sensitive to variations in groundwater recharge and quality.

Geological and structural framework

The geological and structural framework of the Chemora Plain was established primarily from the Geological Map of Algeria, Boulhilet Sheet No. 174, at a scale of 1:50,000, together with the geological cross-sections interpreted from the mapped geological contacts and structural configuration (Figures 2 and 3). The study area is characterized by a central Cretaceous carbonate structural relief, represented by the Fedjoudj–Bouarif ridge, which separates the Chemora–Remila depression to the south from the Chemora–Boulhilet depression to the north. The mapped Cretaceous formations form an uplifted structural high that interrupts the lateral continuity of the Mio-Plio-Quaternary deposits constituting the main shallow aquifer. The geological cross-sections, including the structural section crossing the central relief, show the rise and geometry of the Cretaceous formations and their relationship with the overlying alluvial deposits. These observations provide the

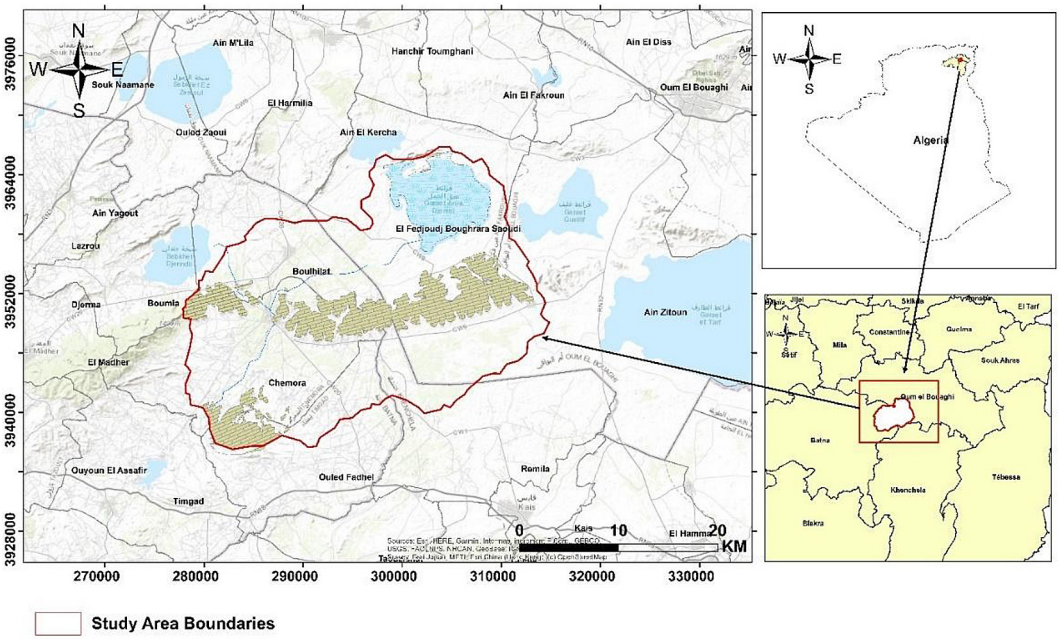

Figure 1. Geographical map of Chemora plain

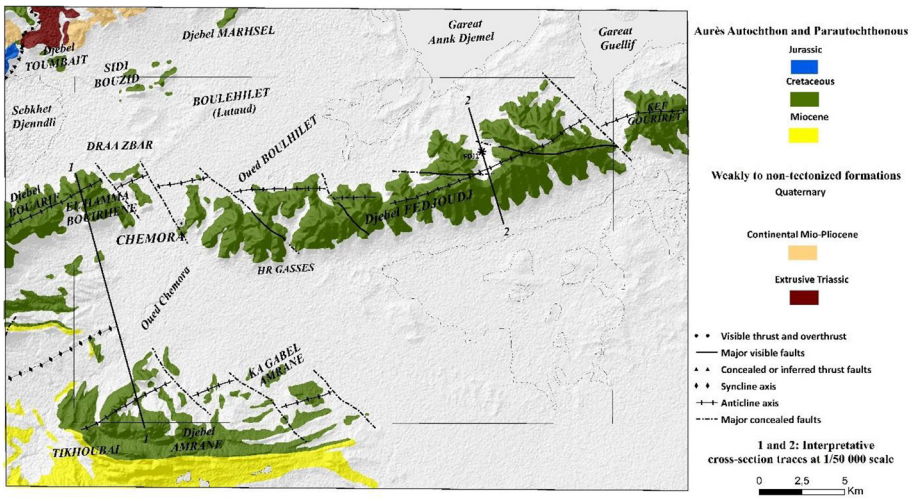

Figure 2. Simplified structural framework of the study area (modified from the Geological Map of Algeria, (Boulhilet Sheet No. 174, scale 1/50 000)

geological basis for interpreting the central relief as a structural threshold controlling the spatial organization of groundwater circulation. The ridge is not continuous along its entire extent: a narrow western discontinuity or breach is visible on the geological map and is also expressed by the cross-sectional configuration. This structural opening is interpreted as a possible zone of localized hydraulic communication between the southern and northern domains.

Hydrogeological context

The Chemora Plain comprises three main groundwater units: the shallow Quaternary aquifer, a Cretaceous carbonate aquifer, and the Mio-Pliocene aquifer associated with the Timgad formations (G.S.A., 1981, 1987). This study focuses on the Quaternary aquifer, which is the main groundwater unit tapped by the sampled wells and widely used for agricultural supply. It consists mainly of gravels, sands, silts and clay-rich deposits overlying Cretaceous carbonate formations. Its thickness varies from approximately 10–20 m in the southern Chemora–Remila sector to about 80 to 100 m in the northern Chemora–Boulhilet sector. The aquifer is predominantly unconfined. (Belkoum, Houha, 2017).

Recharge occurs mainly through precipitation infiltration, with additional local contributions from surrounding carbonate formations and surface runoff. Groundwater flow is predominantly south to north, toward the northern discharge area and Sebkha. Groundwater-level data were available for 12 of the 29 sampled points in 2025; where ground and piezometric elevations were available, groundwater depth ranged from approximately 24 to 90 m below ground level. These observations, together with the geological structure of the plain, provide the hydrogeological basis for interpreting groundwater evolution between the southern and northern compartments.

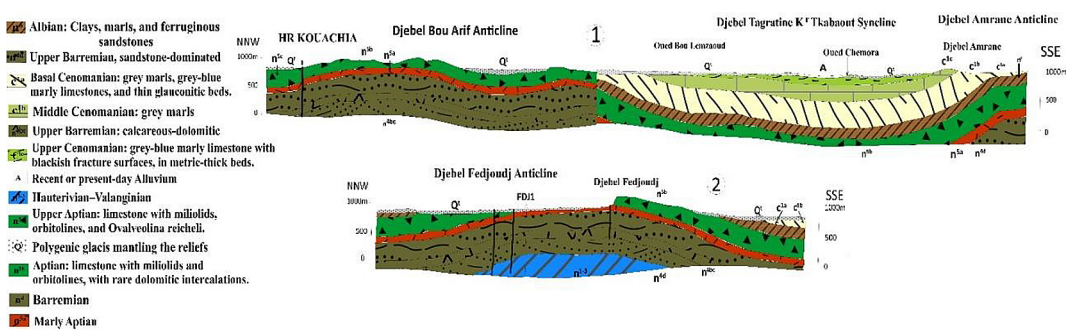

Figure 3. Interpretive geological cross-sections of the Bouarif, Amrane, and Fedjoudj anticlines (modified from the Geological Map of Algeria, Boulhilet Sheet No. 174 [formerly Lutaud], scale 1/50 000)

Groundwater sampling and chemical analysis

A total of 29 groundwater samples were collected from the Chemora aquifer during a field campaign conducted in November 2025 (Figure 4), including 13 samples from the northern compartment and 16 from the southern compartment (Table 1). The sampling network covered the two hydrogeological domains and was designed to represent the principal groundwater-flow direction, lithological variability, and areas subject to different levels of agricultural and anthropogenic influence. The complete sampling metadata, including sample identifiers, compartment assignment, geographic coordinates, ground elevation, and available piezometric levels, are provided in the Supplementary Material (Table S1). Geographic coordinates and ground elevation were recorded using a Garmin eTrex 10 GPS device. Before sampling, each well was purged by pumping at least twice to remove stagnant water and obtain representative groundwater. Samples were filtered on site through 0.45-µm cellulose acetate membranes, collected in precleaned 1-L polyethylene bottles, sealed without headspace, and preserved at 4 °C until laboratory analysis. Piezometric levels measured in 2025 are available for 12 sampling points; for these points, where both ground elevation and piezometric elevation were available, groundwater depth below ground level ranged from approximately 24 to 90 m. Well construction depths and screened or pumping intervals were not consistently documented for all sampling points and were therefore not used as analytical variables in this study. In situ measurements of pH and electrical conductivity (EC; µS cm^{-1}) were performed using a calibrated Hanna HI98130 multiparameter probe. The probe was calibrated before field measurements according to the manufacturer's procedure. In the laboratory, Ca^{2+} and total hardness (TH) were determined by complexometric titration with EDTA, using murexide and Eriochrome Black T (EBT) as indicators, respectively. Mg^{2+} was derived from total hardness and calcium hardness. Cl^- was determined by argentometric titration using $AgNO_3$ and K_2CrO_4 as indicator, whereas HCO_3^- was determined by acid–base titration using H_2SO_4 and methyl orange. NO_3^- and SO_4^{2-} were determined by spectrophotometric methods, whereas Na^+ and K^+ were determined by flame photometry using NaCl and KCl calibration standards, respectively. All laboratory analyses were conducted at the Algerian Water Laboratory (ADE), Batna. Additional information on the analytical procedures, reagents, instruments, and available quality-control documentation is provided in Supplementary Tables S6 and S7.

Analytical quality control / CBE

Analytical quality control was assessed using the charge balance error (CBE), calculated for each sample after converting the major-ion concentrations to meq L^{-1}. The CBE was calculated as:

$$CBE\ (\%) = \frac{(\sum Cations(meq/L) - \sum Anions(meq/L))}{(\sum Cations(meq/L) + \sum Anions(meq/L))} \times 100 \quad (1)$$

A CBE within ±5% was considered indicative of satisfactory ionic balance (Hem, 1985). The overall mean CBE was +4.69%, while mean

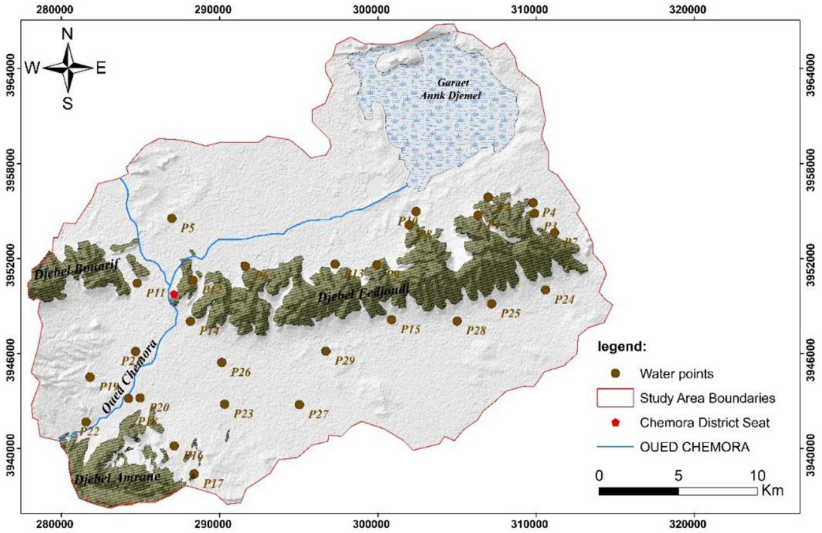

Figure 4. Water point inventory map

Table 1. Physicochemical analysis of groundwater samples in the Chemora Region

Sample	Compa-rtment	pH	EC	Ca	Mg	Na	K	HCO_3	Cl	SO_4	NO_3	THT mg/l	THt mg/l	THp mg/l	$\delta^{18}O$	StD	$\delta^{2}H$	StD	d
			(µS/cm)	(mg/l)								(mg/l $CaCO_3$)			(‰)				
P1	North	6.64	1512	110	73.2	363.2	5.217	336.1	543.8	287.7	30.21	580.00	275.49	304.51	---	---	---	---	---
P2	North	6.76	4560	300.1	124.8	926	15.06	445.7	996.6	764.6	4.08	1270.25	365.33	904.92	---	---	---	---	---
P3	North	6.95	2980	186.7	79.04	424.1	11.57	410.8	677.4	151.2	20.47	796.08	336.72	459.36	-8.3	0.04	-54	0.1	12
P4	North	7.01	4020	230.1	106.1	682.6	13.63	475.5	833.7	518.7	19.31	1017.33	389.75	627.58	---	---	---	---	---
P5	North	7.1	3640	236.7	168.5	546.1	1.884	423.5	667.2	657.2	21.88	1293.83	347.13	946.70	-7	0.05	-49	0.5	7
P6	North	7.19	2430	190.1	89.44	363.2	10.3	364.9	480.4	533.1	37.66	847.92	299.10	548.82	---	---	---	---	---
P7	North	6.84	9180	310.1	129	2007	75.22	928.7	2495	496.8	0.27	1312.75	761.23	551.52	---	---	---	---	---
P8	North	7.03	3840	236.8	139.4	538.2	12.52	440.7	723	448.6	7.62	1172.83	361.23	811.60	-7.7	0.01	-51	0.2	11
P9	North	7.04	4420	286.8	85.28	668	15.53	460.6	958.4	339.4	14	1072.33	377.54	694.79	---	---	---	---	---
P10	North	7.03	5420	413.5	129	210.7	12.04	331.1	1413	205.7	6.11	1571.25	271.39	1299.86	---	---	---	---	---
P11	North	7.27	1821	166.7	58.24	119.3	6.011	374	213	339.2	29.95	659.42	306.56	352.86	-5.9	0.06	-39	0.2	8
P12	North	7.27	2730	220.1	85.28	454.6	10.3	257.3	471.2	502	57.24	905.58	210.90	694.68	---	---	---	---	---
P13	North	7.14	3350	293.4	101.9	302.2	6.011	366	762.1	271.8	17.28	1158.08	300.00	858.08	---	---	---	---	---
P14	South	6.49	2640	220.1	101.9	393.7	9.82	366	423.4	457.4	10.81	974.83	300.00	674.83	-7.5	0.03	-51	0.1	9
P15	South	6.97	3320	313.5	75.92	393.7	3.154	591.4	716.4	217.2	69.11	1100.08	484.75	615.33	---	---	---	---	---
P16	South	6.97	4560	225.1	351	546.1	2.519	400.5	271.1	2362	3.37	2025.25	328.28	1696.97	---	---	---	---	---
P17	South	7.11	4010	556.1	22.31	576.6	2.995	262.6	316.3	1849	91.7	1483.21	215.25	1267.96	-6.7	0.07	-45	0.2	9
P18	South	7.23	1454	113.4	57.2	88.77	2.836	336.8	116.2	400.8	5.17	521.83	276.07	245.77	---	---	---	---	---
P19	South	7.25	2550	201.7	117.5	271.7	2.201	191	245.3	972.5	37.03	993.83	156.56	837.28	---	---	---	---	---
P20	South	7.39	2250	170.1	98.8	149.7	2.042	198.9	129.1	988.8	14.26	836.92	163.03	673.88	---	---	---	---	---
P21	South	7.36	1722	135	90.48	229	3.154	183	135.6	519.1	36.59	714.50	150.00	564.50	-7.3	0.04	-47	0.1	11
P22	South	7.28	3100	291.8	114.4	485.1	4.264	320.9	432.5	1063	32.37	1206.17	263.03	943.13	-6.3	0.05	-43	0.1	8
P23	South	7.15	4350	222.4	202.7	729	1.725	267.9	471.2	1475	60.25	1400.58	219.59	1180.99	---	---	---	---	---
P24	South	6.59	1186	124	50.18	107.1	1.408	339.7	206.5	206.5	15.77	519.08	278.44	240.64	---	---	---	---	---
P25	South	6.82	1645	167.2	45.26	210.7	2.677	308.6	277.6	212.1	20.29	606.58	252.95	353.63	---	---	---	---	---
P26	South	6.91	2020	194.6	84.62	271.7	2.519	481.9	316.3	722.4	30.92	839.08	395.00	444.08	---	---	---	---	---
P27	South	7.11	2420	101	105	543.72	1.884	313.4	542.1	505	14.62	690.00	256.89	433.11	-6.7	0.06	-45	0.1	9
P28	South	7.14	3140	137.2	95.45	469.1	2.519	368.4	458.3	475.2	17.28	740.71	301.97	438.74	-9	0.05	-55	0.2	17
P29	South	7.35	1934	74.14	66.91	393.7	2.201	322.9	471.2	220.7	8.24	464.14	264.67	199.47	---	---	---	---	---

values were +6.00% and +3.62% for the northern and southern compartments, respectively. Individual values ranged from −9.89% to +14.14%. Samples exceeding ±5% were retained because the deviations were considered moderate and because the overall hydrochemical interpretation was supported by independent mineral saturation, stable-isotope and multivariate evidence. Individual CBE values and their assessment are provided in Supplementary Table S1.

Hydrochemical calculations

Electrical conductivity

Electrical conductivity (EC) was measured in situ at the time of sampling using a calibrated Hanna HI98130 multiparameter probe and expressed in µS cm^{-1} at 25 °C. Calibration was performed before the field campaign using standard conductivity solutions according to the instrument manufacturer's procedure. EC was used as a first-order indicator of groundwater mineralization and was interpreted together with major-ion chemistry, hardness, mineral saturation indices and stable isotope data.

Water hardness

Total hardness (TH) was calculated from Ca^{2+} and Mg^{2+} concentrations, expressed in mg L^{-1}, and reported as mg L^{-1} as $CaCO_3$ using the APHA (2017) relationship:

$$THT = 2.497[Ca^{2+}] + 4.118[Mg^{2+}] \quad (2)$$

Carbonate (temporary) hardness (THt), expressed as mg L^{-1} as $CaCO_3$, was calculated directly from bicarbonate concentration according to:

$$THt = [HCO_3^-]/1.22 \quad (3)$$

where: HCO_3^- is expressed in mg L^{-1}.

Non-carbonate (permanent) hardness (THp) was calculated as:

$$THp = THT - THt \quad (4)$$

All calculations were performed automatically using Microsoft Excel (2016) from the measured Ca^{2+}, Mg^{2+}, and HCO_3^- concentrations. The distinction between THt and THp was used to assess the relative contributions of carbonate and non-carbonate components to groundwater mineralization and to compare their spatial hydrochemical evolution between the northern and southern compartments.

Saturation index modelling

Mineral saturation indices (SI) were calculated using PHREEQC version 3 (Parkhurst and Appelo, 2013) with the WATEQ4F thermodynamic database. Calculations were performed for calcite, aragonite, dolomite, gypsum, anhydrite and halite. For each groundwater sample, the PHREEQC input composition was based on pH and the measured concentrations of Ca^{2+}, Mg^{2+}, Na^+, K^+, HCO_3^-, Cl^- and SO_4^{2-}, expressed in mg L^{-1}. Ion activities were calculated using the extended Debye–Hückel activity model implemented in PHREEQC which is appropriate for fresh to moderately mineralized groundwater. Saturation indices were used to assess carbonate equilibrium, evaporite dissolution and the geochemical evolution of groundwater within the two hydrogeological compartments.

Because individual water-temperature measurements were not included in the analytical dataset, no sample-specific temperature correction was applied. SI values were interpreted as thermodynamic indicators of equilibrium state and potential mineral dissolution or precipitation, rather than direct proof of reaction rates.
The saturation index is defined as:

$$SI = \log\left(\frac{IAP}{K}\right) \quad (5)$$

where: IAP is the ion activity product and K is the thermodynamic equilibrium constant of the considered mineral.

An SI value close to zero indicates approximate equilibrium between groundwater and the mineral phase, negative values indicate undersaturation and a thermodynamic potential for mineral dissolution, whereas positive values indicate supersaturation and a thermodynamic tendency toward precipitation.

Stable isotope analysis

Stable isotope analyses were performed on 10 groundwater samples, comprising 4 samples from the northern compartment and 6 samples from the southern compartment. These samples were selected to represent both hydrogeological domains. Water was collected in airtight high-density polyethylene bottles without headspace and stored at 4 °C until analysis. $\delta^{18}O$ and $\delta^{2}H$ were determined by isotope ratio mass spectrometry (IRMS) at the Algiers Nuclear Research Center (CRNA). Results were reported in ‰ relative to VSMOW according to the conventional expression:

$$\delta(\text{ permil }) = \left(\frac{R_{sample}}{R_{VSMOW}} - 1\right) \times 1000 \quad (6)$$

where: R represents the isotope ratio $^{18}O/^{16}O$ or $^{2}H/^{1}H$.

Analytical precision was approximately ±0.1‰ for $\delta^{18}O$ and ±1‰ for $\delta^{2}H$. Deuterium excess was calculated as d-excess = $\delta^{2}H - 8\delta^{18}O$. The GMWL of Craig (1961) was used as the principal meteoric reference, together with regional meteoric-water information where available.

The deuterium excess (d-excess) was calculated following Dansgaard (1964):

$$d = \delta^2 H - 8\delta^{18} O \quad (7)$$

The isotopic data were interpreted with respect to the Global Meteoric Water Line (Craig, 1961) and available Local Meteoric Water Lines in order to identify groundwater origin, recharge conditions and evaporation effects.

Statistical analysis

Descriptive statistics (minimum, maximum, mean, standard deviation and coefficient of variation) and PCA were calculated using XLSTAT 2014.5.03 (Addinsoft, 2014). PCA was performed on standardized variables (zero mean and unit variance) using the Pearson correlation matrix. This method was subsequently applied to identify the dominant hydrogeochemical processes controlling groundwater chemistry and to investigate the influence of geological compartmentalization on groundwater evolution (Singh, 2020; Brahmia et al., 2018). The global PCA used 26 samples and 10 variables: EC, Ca^{2+}, Mg^{2+}, Na^{+}, K^{+}, HCO_3^{-}, Cl^{-}, SO_4^{2-}, THt and THp. A sector-based PCA used the same 10 variables for the northern (n = 13) and southern (n = 13) compartments, represented as separate N and S variables in the same factorial analysis. The first two global components had eigenvalues of 5.297 and 2.773 and explained 52.97% and 27.73% of the variance, respectively (80.70% cumulatively). For the sector-based analysis, F1 and F2 explained 31.88% and 25.09%, respectively (56.97% cumulatively). pH was excluded because of its limited spatial variability, whereas NO_3^{-} was excluded because its variability was considered mainly associated with localized anthropogenic inputs rather than the regional natural geochemical gradient. Components were interpreted from their eigenvalues, explained variance and factor loadings.

The latter analysis was designed to test whether the structural ridge corresponds to differentiated hydrochemical signatures and whether common variable loadings are consistent with partial hydraulic communication.

RESULTS AND DISCUSSION

Structural control on groundwater mineralization

The hydrochemical results indicate that groundwater evolution in the Chemora Plain cannot be explained as the product of a single, homogeneous aquifer. Instead, the geomorphological setting, characterized by the Fedjoudj-Bouarif structural threshold that separates the northern and southern depressions, exerts a primary control on groundwater flow. This structural compartmentalization influences recharge pathways, groundwater residence time, and water–rock interactions, resulting in distinct hydrochemical signatures in the two sectors

Evolution of electrical conductivity

Electrical conductivity (EC) was plotted along the south–north direction to investigate the spatial evolution of groundwater mineralization within the Chemora Plain (Figure 5). The profile reveals differentiated hydrochemical behaviour on either side of the Cretaceous Fedjoudj–Bouarif structural ridge. However, EC values of comparable magnitude occur near the structural boundary, indicating that the two sectors are not completely hydraulically isolated and providing independent support for localized communication across the structural discontinuity.

In the southern compartment, EC values generally decrease northward, indicating progressive dilution of groundwater. This sector corresponds to the principal recharge zone where meteoric water infiltrates through

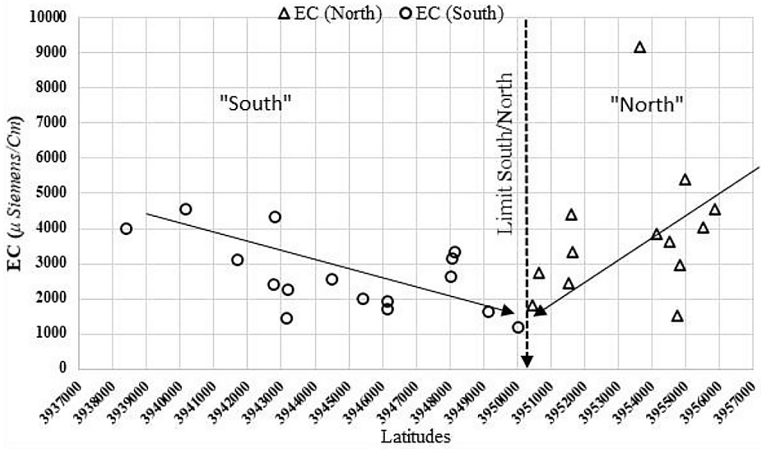

Figure 5. Evolution of the electrical conductivity of water as a function of latitude

fractured carbonate formations and coarse Mio-Plio-Quaternary deposits. Under these conditions, groundwater experiences relatively short residence times and limited water–rock interaction, resulting in comparatively low dissolved salt concentrations.

A pronounced decrease in EC is observed close to the structural boundary separating the two compartments. Rather than indicating complete hydraulic isolation, this local anomaly is interpreted as the influence of less mineralized groundwater circulating preferentially through the western structural breach that interrupts the Cretaceous ridge. This localized hydraulic connection modifies groundwater chemistry near the discontinuity and suggests partial groundwater exchange between the northern and southern sectors.

In contrast, groundwater from the northern compartment exhibits a progressive increase in EC toward the Sebkha area. This evolution reflects continuous groundwater mineralization during northward flow, resulting from prolonged water–rock interaction, dissolution of evaporitic minerals and increasing groundwater residence time. These processes are further enhanced by the semi-arid climatic conditions, where high evapotranspiration rates promote concentration of dissolved salts.

Evolution of groundwater hardness

The spatial evolution of groundwater hardness (total hardness, permanent hardness and temporary hardness) (Figure 6a, 6b 6c) closely follows the electrical conductivity pattern and further confirms the existence of two hydrogeochemically distinct groundwater compartments.

Groundwater within the southern compartment is characterized by relatively low to moderate total hardness dominated by temporary (carbonate) hardness. This hydrochemical signature reflects the predominance of carbonate weathering, mainly involving calcite and dolomite dissolution during the initial stages of groundwater circulation. The predominance of bicarbonate hardness indicates recent recharge conditions and relatively limited groundwater evolution.

A significant decrease in total and permanent hardness is observed near the structural boundary. This behavior coincides with the conductivity minimum previously identified and probably results from localized hydraulic communication through the western structural breach, where less mineralized groundwater partially mixes with groundwater circulating within the northern compartment.

Conversely, groundwater from the northern compartment displays progressively increasing total hardness dominated by permanent hardness.

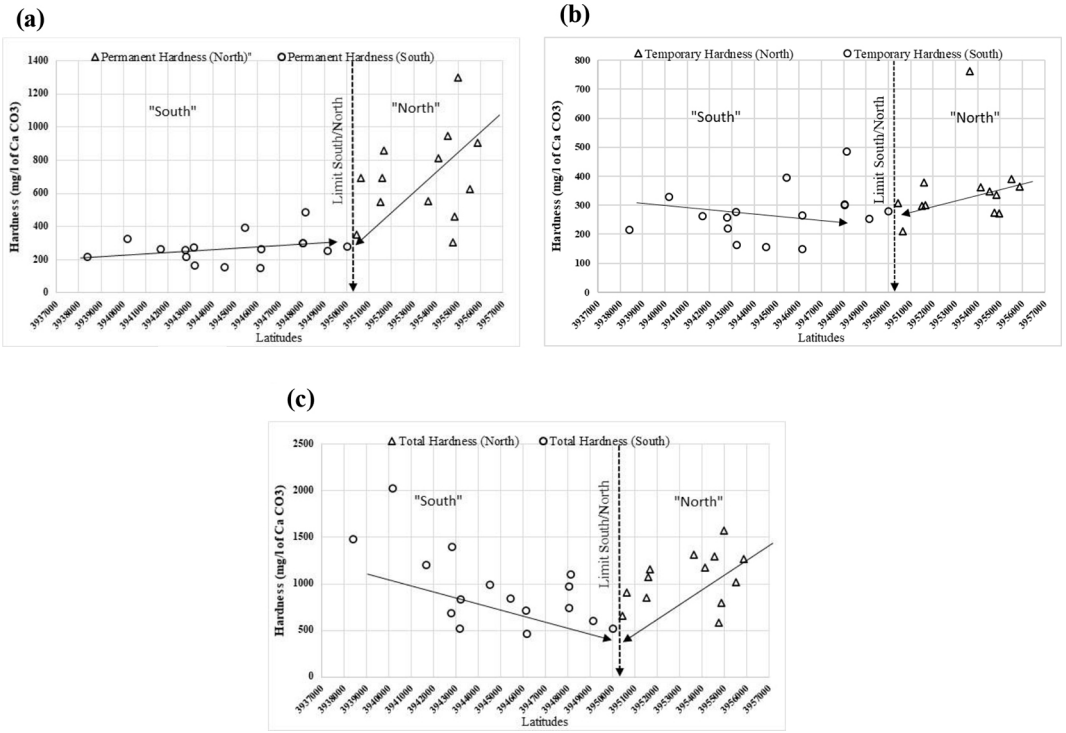

Figure 6. Evolution of water hardness as a function of latitude: (a) total, (b) permanent, (c) temporary

This evolution is associated with increasing sulfate and chloride concentrations generated by evaporite dissolution during prolonged groundwater circulation. Longer residence times, combined with evaporative concentration under semi-arid climatic conditions, progressively transform carbonate hardness into non-carbonate hardness.

The remarkable agreement between conductivity and hardness evolution strongly supports the conceptual hydrogeological model in which groundwater undergoes progressive geochemical evolution from the southern recharge zone toward the northern discharge area while remaining partially influenced by localized hydraulic exchanges across the structural discontinuity.

Water–rock interaction and mineral equilibrium

Southern compartment (recharge area)

The saturation indices calculated using PHREEQC indicate that groundwater in the southern compartment is generally close to equilibrium with carbonate minerals while remaining significantly undersaturated with evaporite minerals (Table 2).

Calcite exhibits a mean saturation index of 0.128, varying between −0.320 and 0.520, whereas aragonite_remains close to equilibrium with a mean value of −0.016. Dolomite presents a mean saturation index of 0.279, with individual values ranging from −0.620 to 0.810. These values indicate that carbonate phases are generally close to equilibrium, consistent with substantial interaction between groundwater and carbonate formations. The SI values alone do not quantify dissolution rates; their significance is strengthened by the observed Ca^{2+}–Mg^{2+}–HCO_3^- chemistry and the geological occurrence of carbonate rocks.

The relatively high carbonate saturation reflects rapid water–rock interaction within the recharge zone, where groundwater residence times remain relatively short but sufficient to establish equilibrium with carbonate minerals. Such conditions are typical of groundwater systems circulating through carbonate terrains under open-system conditions.

In contrast, evaporite minerals remain markedly undersaturated. Mean saturation indices equal −1.027 for anhydrite, −0.807 for gypsum and −5.519 for halite, indicating that groundwater remains thermodynamically capable of dissolving these minerals along the flow path. The particularly low saturation state of halite reflects its high solubility. When considered together with the observed sulfate-, chloride- and sodium-rich compositions, these SI values support a contribution of evaporite dissolution to groundwater mineralization, rather than constituting evidence of dissolution by themselves.

Standard deviations ranging between 0.218 and 0.635 indicate moderate variability in saturation conditions, suggesting relatively homogeneous hydrogeochemical processes throughout the southern compartment despite local lithological variations.

The coexistence of near-equilibrium carbonate minerals and strongly undersaturated evaporites demonstrates that groundwater chemistry within the recharge area is primarily controlled by carbonate weathering, whereas evaporite dissolution remains a secondary process that continues during subsequent groundwater circulation.

Northern compartment (discharge area)

Groundwater within the northern compartment exhibits a more advanced stage of hydrogeochemical evolution than groundwater from the southern recharge area.

The saturation indices calculated (Table 3) noted that calcite presents a mean saturation index of 0.266, aragonite 0.122 and dolomite 0.517, indicating that groundwater progressively approaches carbonate equilibrium during northward circulation. The higher saturation state observed for dolomite reflects increasing groundwater

Table 2. Statistics on saturation indices for the southern zone

Statistic	Aragonite	Calcite	Dolomite	Anhydrite	Gypsum	Halite
Minimum	-0.460	-0.320	-0.620	-1.720	-1.500	-6.610
Maximum	0.380	0.520	0.810	-0.270	-0.050	-3.770
Mean	-0.016	0.128	0.279	-1.027	-0.807	-5.519
Standard deviation	0.218	0.219	0.406	0.353	0.353	0.635
Variation coefficient	-13.508	1.663	1.408	-0.333	-0.424	-0.111

Table 3. Statistics on saturation indices for the northern zone

Statistic	Aragonite	Calcite	Dolomite	Anhydrite	Gypsum	Halite
Minimum	-0.600	-0.460	-0.750	-1.570	-1.350	-6.220
Maximum	0.320	0.460	0.850	-0.860	-0.640	-4.030
Mean	0.122	0.266	0.517	-1.159	-0.941	-5.134
Stand dev	0.244	0.245	0.435	0.192	0.191	0.490
Var coef	1.927	0.883	0.808	-0.159	-0.195	-0.092

residence time and continued interaction with carbonate formations.

Despite the higher degree of mineralization observed in this compartment, groundwater remains undersaturated with respect to evaporite minerals. Mean saturation indices reach −1.159 for anhydrite, −0.941 for gypsum and −5.134 for halite. These values indicate that the groundwater remains thermodynamically capable of further interaction with evaporite phases. Their interpretation, combined with the enrichment of SO_4^{2-}, Cl^- and Na^+ and the geological setting, supports the continued contribution of evaporite dissolution to the progressive mineralization of groundwater during circulation.

The persistence of evaporite undersaturation despite increasing groundwater salinity indicates that evaporite dissolution represents a continuous geochemical process accompanying groundwater circulation rather than a process limited to recharge areas. Simultaneously, evaporation progressively concentrates dissolved constituents without modifying the thermodynamic tendency toward continued evaporite dissolution.

The relatively low standard deviations recorded for all minerals indicate moderate spatial variability and suggest that similar hydrogeochemical processes dominate throughout the northern compartment.

Overall, groundwater from the northern compartment represents a more evolved hydrochemical stage characterized by prolonged groundwater circulation, enhanced water–rock interaction and progressive concentration of dissolved salts prior to discharge toward the Sebkha system.

Hydrogeochemical significance of saturation indices

Comparison between the two hydrogeological compartments reveals a progressive geochemical evolution of groundwater along the regional south–north flow path.

Groundwater rapidly reaches equilibrium with carbonate minerals shortly after infiltration because calcite and dolomite dissolve relatively rapidly under natural groundwater conditions. Conversely, gypsum, anhydrite and particularly halite remain undersaturated throughout the aquifer owing to their considerably higher solubility.

The gradual increase in carbonate saturation observed from south to north therefore reflects increasing groundwater residence time rather than carbonate precipitation. Likewise, the persistent undersaturation of evaporite minerals demonstrates that groundwater continuously dissolves these minerals during circulation. These results indicate that groundwater mineralization within the Chemora aquifer is governed by the combined effects of carbonate weathering, evaporite dissolution and evaporative concentration. The saturation indices therefore provide independent evidence supporting the hydrogeological interpretation previously established from conductivity and hardness evolution.

Stable isotope evidence of groundwater recharge and evolution

Isotopic composition

The statistical characteristics of stable isotope data indicate relatively limited isotopic variability throughout the Chemora aquifer (Table 4). Groundwater $\delta^{18}O$ values range from −8.96‰ to −5.89‰, with a mean value of −7.22‰, whereas $\delta^{2}H$ values vary between −54.98‰ and −39.10‰, averaging −47.90‰. The relatively narrow isotopic ranges suggest that groundwater throughout the study area originates from a common recharge source despite the hydrochemical contrasts observed between the two structural compartments.

The calculated deuterium excess (d-excess) varies between 7‰ and 17‰, with an average value of 10.1‰, very close to the theoretical

Table 4. Statistics of the isotopes of the water molecule $\delta^{18}O$ and $\delta^{2}H$

Statistic	$\delta^{18}O$	$\delta^{2}H$	d
Minimum	-8.960	-54.980	7.00
Maximum	-5.890	-39.100	17.00
Mean	-7.223	-47.898	10.10
Standard deviation	0.922	5.125	2.885
Variation coefficient	-0.121	-0.102	0.271

value proposed for global meteoric precipitation. This observation indicates that groundwater recharge is predominantly derived from meteoric precipitation and has undergone only limited isotopic modification before infiltration.

The standard deviations of 0.92‰ for $\delta^{18}O$ and 5.13‰ for $\delta^{2}H$ indicate moderate isotopic dispersion, whereas the relatively low coefficients of variation confirm the overall isotopic homogeneity of the aquifer. Such characteristics suggest that groundwater chemistry is controlled primarily by subsurface geochemical processes rather than by major differences in recharge origin.

Interpretation of the $\delta^{18}O$–$\delta^{2}H$ relationship

The relationship between $\delta^{18}O$ and $\delta^{2}H$ provides valuable information regarding groundwater origin and subsequent evolution (Figure 7). Most groundwater samples plot close to the global meteoric water line (GMWL) established by Craig (1961), indicating that recharge is mainly derived from direct infiltration of meteoric precipitation.

A limited number of samples exhibit a slight displacement below the meteoric water line, reflecting moderate isotopic enrichment produced by evaporation prior to or during infiltration.

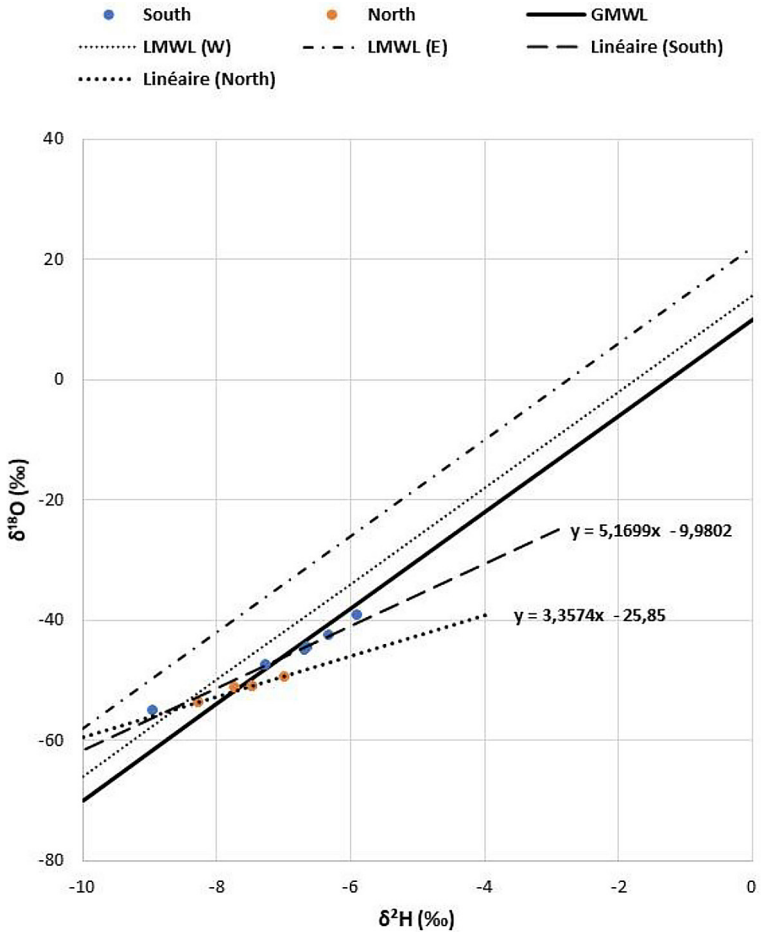

Figure 7. Global, regional, and groundwater δ18O/δ2H relationship

Such behavior is characteristic of semi-arid environments where precipitation infiltrates under elevated temperatures and intense evapotranspiration. Nevertheless, the magnitude of this enrichment remains relatively small, demonstrating that evaporation has only a minor influence on the isotopic composition of groundwater.

The similarity of isotopic signatures observed in both the northern and southern compartments demonstrates that the Cretaceous structural ridge does not separate groundwater derived from different recharge sources. Instead, both compartments receive recharge from the same regional meteoric system, while their contrasting hydrochemical characteristics develop after recharge through differences in groundwater circulation, residence time and water–rock interaction.

The absence of strongly enriched isotopic compositions further indicates that groundwater does not experience significant evaporation after infiltration. Consequently, the progressive increase in groundwater salinity observed toward the northern compartment cannot be explained solely by evaporative concentration. Rather, it mainly results from prolonged groundwater circulation through carbonate and evaporitic formations, where continuous mineral dissolution progressively enriches groundwater in dissolved ions.

Deuterium excess

The distribution of d-excess values provides additional insight into recharge conditions within the Chemora aquifer. Most groundwater samples display d-excess values ranging between 9‰ and 11‰, closely matching the average value of modern meteoric precipitation. These results indicate recharge under climatic conditions comparable to those currently prevailing in northeastern Algeria.

Samples exhibiting slightly lower d-excess values (approximately 7–8‰) probably reflect minor evaporation of infiltrating water before recharge, whereas values exceeding 15‰ may indicate seasonal variations in precipitation or recharge occurring under relatively low atmospheric humidity.

Overall, the relatively narrow range of d-excess values confirms that groundwater recharge has been only slightly affected by evaporation and retains a predominantly meteoric isotopic signature. These observations are fully consistent with the $\delta^{18}O$–$\delta^{2}H$ relationship and reinforce the conclusion that evaporation is not the principal mechanism responsible for groundwater mineralization within the Chemora Plain.

Hydrogeological implications of stable isotopes

The integration of stable isotope data with hydrochemical and geological observations provides a coherent conceptual interpretation of groundwater functioning within the Chemora Plain.

Groundwater recharge mainly occurs over the southern part of the plain and along the surrounding carbonate highlands, where meteoric water infiltrates through fractured carbonate rocks and permeable alluvial deposits. After infiltration, groundwater flows northward through the Quaternary aquifer while progressively interacting with carbonate and evaporite minerals.

Although the Fedjoudj-Bouarif Cretaceous ridge structurally divides the plain into two hydrogeological compartments, the similarity of isotopic signatures on both sides of the structural boundary demonstrates that both compartments originate from the same regional recharge system. The observed hydrochemical differences therefore reflect distinct groundwater residence times and water–rock interaction intensities rather than different recharge sources.

The western structural breach probably facilitates localized groundwater exchange between both compartments, explaining the convergence of hydrochemical characteristics observed near the structural discontinuity without modifying the general isotopic composition of groundwater.

Consequently, stable isotope evidence independently validates the conceptual hydrogeological model proposed in this study, confirming that structural compartmentalization primarily controls groundwater evolution while exerting only a limited influence on groundwater recharge.

Principal component analysis

Global hydrochemical controls

PCA (Figure 8) was performed to identify the principal factors controlling groundwater chemistry and to evaluate the influence of structural compartmentalization on groundwater evolution within the Chemora aquifer. The analysis incorporated the major physicochemical parameters, major ions and hardness components. Variables were standardized prior to analysis. The interpretation

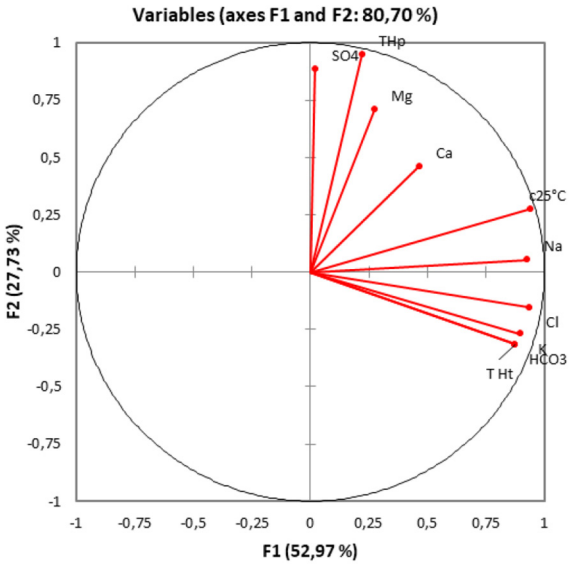

Figure 8. PCA circle of overall analysis results of Chemora waters: THt – temporary hardness, THp – permanent hardness, c25 °C – electrical conductivity

focuses on the magnitude and direction of variable loadings and on the proportion of total variance represented by the retained axes.

The first two principal components explain most of the total variance, indicating that groundwater chemistry is governed by a limited number of dominant hydrogeochemical processes.

The first principal component (PC1) mainly represents the groundwater mineralization gradient. Strong positive loadings are associated with electrical conductivity, sodium, chloride, sulfate, magnesium and permanent hardness, reflecting progressive mineralization and the combined influence of water–rock interaction and evaporite-related solute acquisition. The second principal component (PC2) is associated mainly with bicarbonate, calcium and temporary hardness, representing the carbonate-weathering and recharge-related component of groundwater evolution.

Principal component analysis of the northern and southern compartments

A single PCA was performed using the hydrochemical variables of the northern (N) and southern (S) compartments (Figure 9). The first two components explain 56.97% of the total variance, with F1 accounting for 31.88% and F2 for 25.09%. The factorial plane shows a clear differentiation between the two sectors, with most southern variables distributed toward the negative side of F1, whereas the northern variables are mainly associated with its positive side.

In the southern compartment, the association of HCO_3^-(S), THt(S), Mg(S), Na(S) and Cl(S) indicates an important contribution of carbonate weathering and water–rock interaction. In contrast, the northern compartment is characterized by the close association of EC(N), Na(N), Cl(N), SO_4(N), HCO_3(N) and hardness parameters, reflecting a stronger mineralization signal and a greater contribution of mineral dissolution along groundwater circulation.

The partial overlap of some variables, particularly Ca, SO_4 and hardness, indicates that the two compartments are not completely independent. This statistical pattern is consistent with the geological structure of the plain, where the Cretaceous Fedjoudj–Bouarif ridge acts as a major hydrogeological threshold while the western structural breach may permit localized hydraulic communication between the northern and southern compartments. Overall, the PCA supports a differentiated but partially connected hydrogeological functioning, with distinct hydrochemical evolution in the two compartments rather than complete hydraulic isolation.

Hydrogeological significance of the PCA

The PCA provides statistical support for the conceptual hydrogeological model proposed for the Chemora Plain. The spatial differentiation of the variables on the factorial plane is consistent

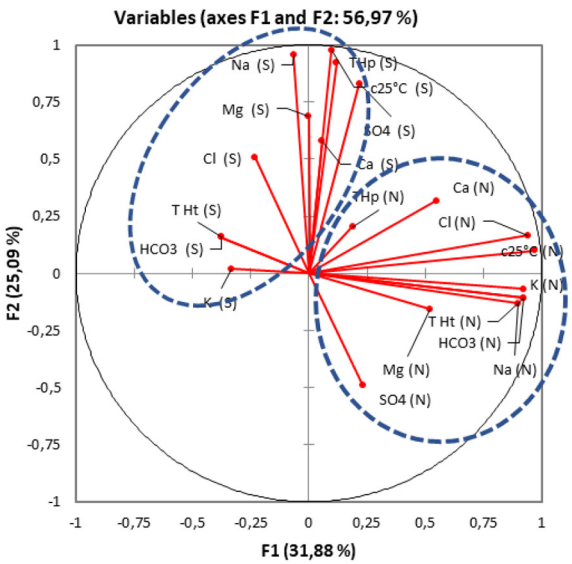

Figure 9. Principal component analysis (PCA) of hydrochemical variables measured in the northern (N) and southern (S) compartments of the Chemora Plain

with the geological evidence showing that the Cretaceous ridge constitutes a structural threshold between the northern and southern depressions.

However, the PCA should not be interpreted as evidence of complete hydraulic isolation. The presence of common hydrochemical variables in intermediate positions, particularly Ca, SO_4 and THp, indicates that some processes affect both sectors. This partial convergence is consistent with the existence of hydraulic communication across the structural discontinuity identified in the western part of the ridge.

The PCA therefore supports a model in which the northern and southern sectors represent hydrochemically differentiated but hydraulically connected compartments, rather than two completely independent aquifers.

Integrated hydrogeological model

The integration of geological, hydrochemical, isotopic and statistical evidence allows the development of a comprehensive conceptual model describing groundwater circulation within the Chemora Plain (Figure 10).

Groundwater recharge predominantly occurs over the carbonate highlands bordering the southern part of the basin and through direct infiltration across permeable Mio-Plio-Quaternary deposits. Recharge waters are initially characterized by low mineralization and a calcium–magnesium–bicarbonate hydrochemical facies resulting from carbonate dissolution. During this early stage of groundwater evolution, carbonate minerals rapidly approach equilibrium, whereas evaporite minerals remain strongly undersaturated.

The east–west-oriented Fedjoudj-Bouarif Cretaceous ridge constitutes the principal structural feature controlling groundwater circulation. This uplifted carbonate structure interrupts the lateral continuity of the alluvial aquifer and divides the Chemora Plain into two hydrogeological compartments exhibiting distinct groundwater evolution pathways. Nevertheless, a narrow tectonic breach located in the western part of the ridge provides localized hydraulic connectivity, allowing partial groundwater exchange between both compartments.

Following recharge, groundwater progressively migrates northward toward the Sebkha

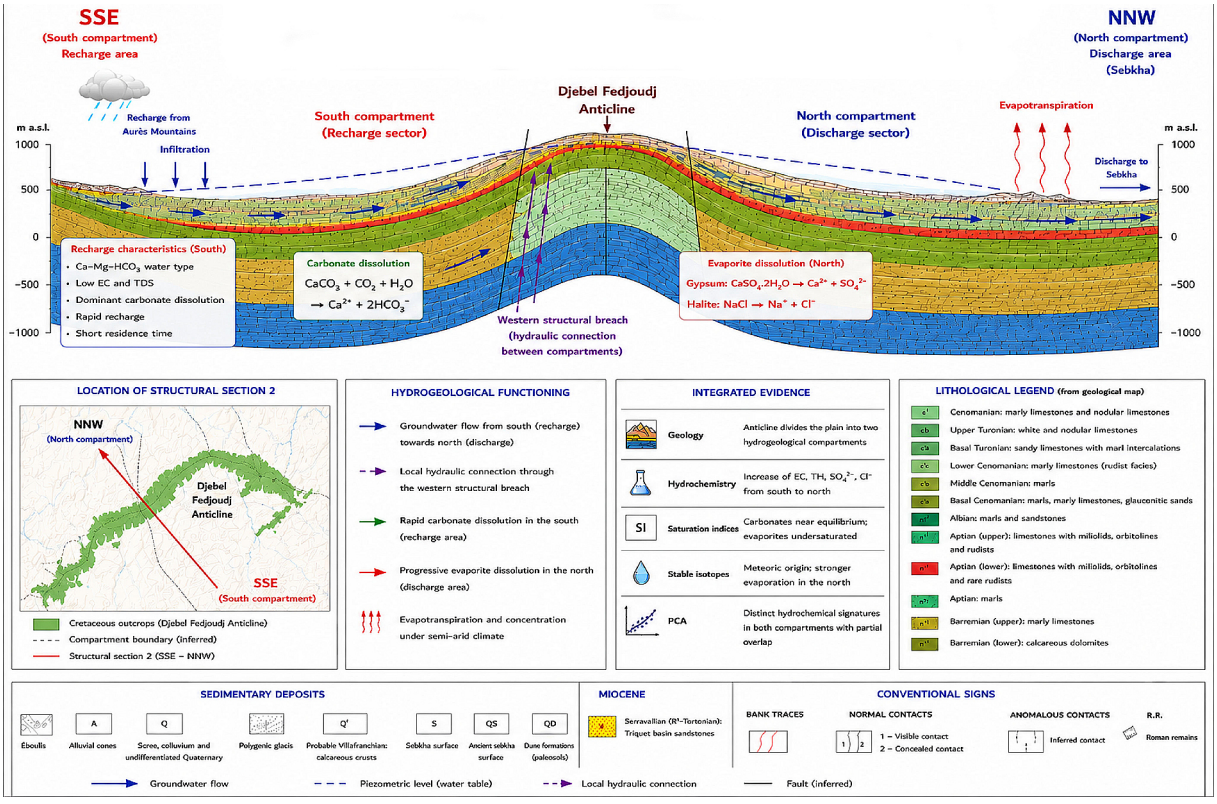

Figure 10. Conceptual hydrogeological model of groundwater circulation in the Chemora plain controlled by the Djebel FEDJOUDJ anticline "Conceptual model developed by the authors based on the integrated geological, hydrochemical, isotopic and statistical results"

discharge zone. Along this flow path, increasing residence time promotes continued dissolution of gypsum, anhydrite and halite, leading to gradual increases in electrical conductivity, sulfate, chloride, sodium, magnesium and permanent hardness. Simultaneously, high evapotranspiration rates characteristic of the semi-arid climate further concentrate dissolved constituents without significantly modifying the isotopic composition of groundwater.

Stable isotope data indicate that groundwater in both compartments shares a predominantly meteoric origin, with $\delta^{18}O$ values ranging from −8.96 to −5.89‰, $\delta^{2}H$ from −54.98 to −39.10‰ and d-excess from 7 to 17‰. The observed hydrochemical contrasts are therefore interpreted primarily in terms of differences in groundwater circulation, residence time and water–rock interaction rather than as evidence for fundamentally different recharge sources. PCA independently supports the distinction between recharge-related and mineralization-related hydrochemical associations.

Overall, the proposed conceptual model demonstrates that groundwater evolution within the Chemora Plain is governed by the combined influence of structural compartmentalization, groundwater flow dynamics, carbonate weathering, evaporite dissolution and semi-arid climatic conditions. The remarkable convergence of geological observations, hydrochemical analyses, saturation indices, stable isotope data and multivariate statistics provides a robust framework for understanding groundwater functioning and offers valuable scientific support for the sustainable management of groundwater resources in this vulnerable agricultural basin.

These findings also have broader implications for water-resource management in semi-arid regions, where understanding hydrological controls is essential for developing sustainable strategies under increasing climatic and anthropogenic pressures (Noor et al., 2025). In addition the results obtained emphasize the importance of appropriate water-quality protection and treatment strategies for sustainable water-resource management (Zahorodniuk, K. et al, 2019).

CONCLUSIONS

This study provides an integrated assessment of groundwater evolution in the Chemora Plain by combining geological and structural information with hydrochemical, mineral-saturation, stable-isotope and multivariate evidence. The results demonstrate a clear hydrochemical differentiation between the southern recharge domain and the northern discharge domain, with groundwater evolving along a predominantly south–north flow path.

The Fedjoudj–Bouarif Cretaceous ridge represents a major structural threshold that interrupts the lateral continuity of the Quaternary aquifer and coincides with a marked differentiation in electrical conductivity, hardness and major-ion composition. Groundwater in the southern compartment is characterized by lower to moderate mineralization and a stronger carbonate contribution, whereas the northern compartment shows a more evolved chemical signature associated with increasing mineralization and a greater contribution from non-carbonate components.

Mineral saturation modelling indicates that carbonate minerals remain close to equilibrium in both compartments, whereas gypsum, anhydrite and halite remain undersaturated. When considered together with the major-ion chemistry, these results indicate that carbonate water–rock interaction is important during the early stages of circulation, while continued interaction with evaporitic minerals contributes to the progressive acquisition of dissolved solutes along the groundwater flow path. The increasing mineralization toward the northern discharge zone therefore cannot be attributed to evaporation alone. Stable isotope compositions, with $\delta^{18}O$ values ranging from −8.96 to −5.89‰, $\delta^{2}H$ values from −54.98 to −39.10‰, and d-excess values from 7 to 17‰, indicate a predominantly meteoric recharge source with limited isotopic modification. The similarity of isotopic signatures between the two compartments suggests a common regional recharge system, while the observed hydrochemical contrasts mainly reflect differences in groundwater circulation, residence time and water–rock interaction.

The PCA further confirms the existence of differentiated hydrochemical signatures in the northern and southern sectors, while the partial overlap of several variables indicates that the two compartments are not completely hydraulically isolated. The western structural breach therefore represents a plausible zone of localized hydraulic communication across the Cretaceous ridge. Overall, the convergence of geological, hydrochemical, isotopic and statistical evidence demonstrates that structural organization exerts a first-order control on groundwater evolution in the Chemora Plain, while

allowing limited hydraulic exchange between the two compartments. These findings provide a coherent basis for understanding groundwater mineralization in this semi-arid agricultural basin and highlight the importance of incorporating geological structures, groundwater-flow organization and geochemical evolution into long-term groundwater management and protection strategies.

Acknowledgements

The authors would like to express their sincere gratitude to the staff of the Laboratory of Water Resources Mobilization and Management (LMGRE), University of Batna 2, for their valuable support throughout this study. They also wish to thank the authorities of the Batna Province, the National Agency for Hydraulic Resources (ANRH), the Directorate of Water Resources (DRE) and its local subdivisions, and the Laboratory of the Algerian Water Company (ADE), Batna, for their cooperation and assistance during field investigations. The authors are also grateful to the Algiers Nuclear Research Center (CRNA) for performing the isotopic analyses that contributed to this research.

REFERENCES

1. Addinsoft. (2014). XLSTAT (Version 2014.5.03) [Logiciel].
2. Ali, N., Kausar, A., Vambol, S., Kozub, P., Kozub, S. (2024). Environmental retrieval during COVID-19 lockdown in the megacity Karachi, Pakistan. *Ecological Questions, 35*(3), 1–16. https://doi.org/10.12775/EQ.2024.032
3. Aouidane L., Belhamra M., Kheddouma A. (2021). Integrated statistical and hydro-geochemical approach to identify the origin and process of saline contamination of Remila plain groundwater (Khenchela, Algeria). *Earth and Environmental Science Transactions of the Royal Society of Edinburgh*, *112*(2), 89–99. https://doi.org/10.1017/S1755691021000207
4. APHA (2017). *Standard Methods for the Examination of Water and Wastewater (23rd ed.)*. Washington DC: American Public Health Association.
5. Appelo, C.A.J., Postma, D. (2004). *Geochemistry, Groundwater and Pollution (2nd ed.)*. CRC Press. https://doi.org/10.1201/9781439833544
6. Belkoum, N., Houha, B. (2017). Hydrochemistry and isotopic geochemistry contribution to the characterization of the aquifers of the upper Plains of Algeria, case of the basin of Chemora, oriental Algeria. *Journal of Materials and Environmental Science, 8*, 3262–3268.
7. Bezai, A., Brinis, N., Reghais, A., Djenba, S., Bouzid, K. (2024). Hydrochemical analysis and groundwater quality assessment for irrigation in the Remila Plain, Khenchela, Northeast Algeria. *Geomatics, Landmanagement and Landscape,* (3). https://doi.org/10.15576/GLL/2024.3.03
8. Brahmia A., Brinis N., Nouar T. (2018). Statistical and hydrogeochemical characteristics of the M'Daourouch--Drea Plain's groundwater, North-East of Algeria. *Journal of Water and Land Development*, 38, 19–26. https://doi.org/10.2478/jwld-2018-0038
9. Brinis, N., Brahmia, A., Hamel A., Benhamida, S. (2021). Origin and dynamics of the ions controlling the mineralization of spring waters in the upstream part of the Oued Labiod Valley (Western Batna, Algeria): The Ichemoul, Arris, T'Kout, and Ghassira regions. LHB, 107(1), 1–10. (in French), https://doi.org/ 10.1080/27678490.2021.1974285.
10. Brinis, N., Boudoukha, A., Hamel, A. (2015). Statistical and geochemical analysis of the dynamics of the physicochemical parameters of groundwater in the Ghassira Syncline, Eastern Algeria. *Larhyss Journal, 22* (June), 123–137. (in French) http://larhyss.net/ ojs/index.php/larhyss/article/view/282
11. Clark, I., Fritz, P. (1997). *Environmental isotopes in hydrogeology*. CRC Press.
12. Cloutier, V., Lefebvre, R., Therrien, R., Savard, M. M. (2008). Multivariate statistical analysis of geochemical data as indicative of the hydrogeochemical evolution of groundwater in a sedimentary rock aquifer system. *Journal of Hydrology, 353*(3–4), 294–313. https://doi.org/10.1016/j.jhydrol.2008.02.015
13. Craig, H. (1961) Isotopic variations in meteoric waters. *Science, 133*, 1702–1703. https://doi.org/10.1126/science.133.3465.1702
14. Dansgaard, W. (1964), Stable isotopes in precipitation. *Tellus, 16*: 436–468. https://doi.org/10.1111/j.2153-3490.1964.tb00181.x
15. Drever, J. I. (1997). *The geochemistry of natural waters: Surface and groundwater environments (3rd ed.)*. Prentice Hall. ISBN: 0132727900, 9780132727907. 436 pages
16. Esri. (2020). *ArcGIS Desktop 10.8*. Environmental Systems Research Institute, Redlands, CA, USA.
17. Famiglietti, J. S. (2014). The global groundwater crisis. *Nature Climate Change, 4*(11), 945–948. https://doi.org/10.1038/nclimate2425
18. Freeze, R.A., Cherry, J.A. (1979). *Groundwater.* Prentice-Hall, Englewood Cliffs, New Jersey, 604 pp.
19. G.S.A (Geological Survey of Algeria). (1981). *Geological Map of Batna at a Scale of 1:200,000* (in French). Ministry of Energy and Mines, Algeria.

20. G.S.A (Geological Survey of Algeria). (1987). *Explanatory Notes for the Geological Map of Batna* (in French). Ministry of Energy and Mines, Algeria.
21. Ghodbane, M., Boudoukha, A., Benaabidate, L. (2016). Hydrochemical and statistical characterization of groundwater in the Chemora area, northeastern Algeria, *Desalination and Water Treatment Journal, 57*(32), 14858–14868, https://doi.org/10.1080/19443994.2015.1067924
22. Ghodbane, M. (2018). *Assessement of Groundwater Potential and Nitrate Pollution in the Chemora Region, Eastern Algeria.* PhD Thesis. University of Batna2, Batna, Algeria.
23. Gumbo, N., Kapenge, C. (2025). Groundwater contaminated with heavy metals as a threat to population safety and health in developing countries: A scoping review. *Trends in Ecological and Indoor Environmental Engineering, 3*(2), 37–45. https://doi.org/10.62622/TEIEE.025.3.2.37-45
24. Hammadi, A, Brinis N., Djidel, M (2022): Hydrogeochemical behavior associated with a diverse etiology of high salinity in phreatic water along Oued Righ valley in Algerian Sahara. *Arab J Geosci 15, 1168*(2022). https://doi.org/10.1007/s12517-022-10402-0
25. Hardie, L. A., Eugster, H. P. (1970). *The evolution of closed-basin brines.* In B. A. Morgan (Ed.), Mineralogical Society of America Special Paper (Vol. 3, pp. 273–290).
26. Hem, J. D. (1985*). Study and interpretation of the chemical characteristics of natural water (3rd ed.)*. U.S. Geological Survey Water-Supply Paper 2254.
27. Kendall, C., McDonnell, J. J. (Eds.). (1998). *Isotope tracers in catchment hydrology. Amsterdam, The Netherlands*: Elsevier.
28. Noor, S., Salman, A., Alam, F., Bo, D., Ali, B., Khan, G. D., Shahid, R. (2025). Environmental assessment of the Auxiliary Kandar Dam and its influence on the lifespan extension of the Main Reservoir: Evidence from Kohat, Pakistan. *Trends in Ecological and Indoor Environmental Engineering, 3*(4), 12–22. https://doi.org/10.62622/TEIEE.025.3.4.12-22
29. Parkhurst, D., Appelo, T. (2013). *Description of input and examples for PHREEQC version 3 – a computer program for speciation, batch-reaction, one-dimensional transport, and inverse geochemical calculations.* US Geological Survey Techniques and Methods, book 6, chap A43, p 497. http://pubs.usgs. gov/tm/06/a43
30. Rezig A, Mansour D, Saggai S. (2023). Groundwater quality assessement of the northern region of the Middle Sébaou in Algeria, using water quality index and multivariate analysis. *Ecological Engineering & Environmental Technology, 24*(7), 148–153. https://doi.org/10.12912/27197050/169878.
31. Scanlon, B. R., Ruddell, B. L., Reed, P. M., Hook, R. I., Zheng, C., Tidwell, V. C. and Siebert, S. (2017). The food-energy-water nexus: Transforming science for society, *Water Resour. Res., 53*, 3550–3556, https://doi.org/10.1002/2017WR020889
32. Simler, R. (2012). *Software 'Diagrammes'.* Laboratoire d'Hydrologie d'Avignon, Université d'Avignon et pays du Vaucluse, France. http://www.lha.univ-avignon.fr
33. Singh G., Rishi M.S., Herojeet R., Kaur L., Priyanka, Sharma K. (2020). Multivariate analysis and geochemical signatures of groundwater in the agricultural dominated taluks of Jalandhar district, Punjab, India. *Journal of Geochemical Exploration 208*, 106395.
34. Taylor, R. G., Scanlon, B., Döll, P., Rodell, M., van Beek, R., Wada, Yoshihide, Longuevergne, L., Leblanc, M., Famiglietti, J. S., Edmunds, M., Konikow, L., Green, T. R., Chen, J., Taniguchi, M., Bierkens, M. F. P., MacDonald, A., Fan, Y., Maxwell, R. M., Yechieli, Y., Gurdak, J. J., Allen, D. M., Shamsudduha, M., Hiscock, K., Yeh, Pat J.-F., Holman, I., Treidel, H. (2013). Ground water and climate change. *Nature Climate Change, 3*(4), 322–329. https://doi.org/10.1038/nclimate1744
35. UNESCO. (2022). *The United Nations world water development report 2022: Groundwater – Making the invisible visible*. UNESCO Publishing.
36. Yan, J.P., Hinderer, M., Einsele, G. (2002). Geochemical evolution of closed-basin lakes: general model and application to Lakes Qinghai and Turkana., *Sedimentary Geology 148*(1–2), 105–122. https://doi.org/10.1016/s0037-0738(01)00212-3
37. Zahorodniuk, K., Voitsekhovsky, V., Korobochka, A., Hrynzovskyi, A., Averyanov, V. (2019). Development of modernized paper filtering materials for water purification, assessment of their properties. *Eastern-European Journal of Enterprise Technologies, 1*(10(97), 6–13. https://doi.org/10.15587/1729-4061.2019.156534